

## **Second generation prototype design and testing for a high altitude Venus balloon**

J. L. Hall (1), V. V. Kerzhanovich (1), A. H. Yavrouian (1), G. A. Plett (1), M. Said (2), D. Fairbrother (2), C. Sandy (3), T. Frederickson (3), G. Sharpe (3), and S. Day (4)

(1) Jet Propulsion Laboratory, California Institute of Technology, Pasadena, CA, United States

(2) NASA Wallops Flight Facility, Wallops Island, VA, United States

(3) ILC Dover Inc, Frederica, DE, United States

(4) Structural Integrity Associates, Inc., San Jose, CA, United States

### **Abstract**

This paper describes the development of a second generation prototype balloon intended for flight in the upper atmosphere of Venus. The design of this new prototype incorporates lessons learned from the construction and testing of the first generation prototype, including finite element analyses of the balloon stresses and deformations, measured leak performance after handling and packaging, permeability and optical property measurements on material samples, and sulfuric acid testing. An improved design for the second generation prototype was formulated based on these results, although the spherical shape and 5.5 m diameter size were retained. The resulting balloon has a volume of 87 m<sup>3</sup> and is capable of carrying a 45 kg payload at a 55 km altitude at Venus. The design and fabrication of the new prototype is described, along with test data for inflation and leakage performance.

**Keywords:** aerobot, balloon, Venus, mobility

---

### **Introduction**

In 2006, a team of JPL, NASA Wallops and ILC Dover engineers designed, fabricated and tested a full scale, 5.5 m diameter spherical superpressure balloon suitable for flight at a 55 km altitude at Venus (Hall et al, 2007). This successful effort constituted a proof-of-concept demonstration that a large Venus balloon was feasible for carrying a 45 kg payload for multiple days at this altitude. As such, it represented the next step beyond the two Soviet VEGA balloons (Kremnev et al, 1986) that flew at Venus in 1985, but with a much smaller 7 kg payload each. This new balloon design was used as the basis for a flight mission proposal to the NASA Discovery program in 2006, a proposal that featured a scientific investigation of the Venusian atmosphere using a gas chromatograph, mass spectrometer and other instruments on a multi-day flight around the planet. This proposal was not accepted for implementation, although the balloon component itself received generally favorable feedback from the review board.

In anticipation of a future re-proposal of this mission concept, JPL initiated a continued Venus balloon technology development activity aimed at further reducing the technical risk for implementing a Venus balloon on a flight mission. This work had four main elements:

1. Extensive laboratory testing of the Venus balloon material to better characterize its mechanical, thermal and chemical (acid resistance) performance.
2. Detailed finite element analysis of the balloon to better quantify the structural safety margin and reveal areas for design improvements.
3. Sulfuric acid immersion testing on balloon prototypes to verify multi-day integrity.
4. Design, fabrication and testing of a new 5.5 m spherical superpressure balloon that incorporates all of the lessons learned to date.

This paper will describe the results achieved in all four of these elements.

### Balloon Material Thermo-mechanical and Optical Testing

Measured stress-strain curves for the balloon material were presented in the previous paper (Hall et al, 2007). Room temperature tests were repeated in preparation for the second prototype and showed lower tensile strength in the machine direction, 52.1 kN/m vs 71 kN/m and slightly lower strength in the transverse direction, 54.8 kN/m vs 57 kN/m. New structural tapes were used in the new prototype, in which the previous polyester fabric was replaced with a layer of the same Vectran fabric as used in the balloon gores. As before, this fabric is sandwiched between layers of polyurethane coating to promote good adhesion to the gores during fabrication of the balloon. The room temperature stress-strain curves for this new structure tape are shown in Fig. 1. Note that the ultimate tensile strength of the new seam is comparable to the previous one, 58.4 kN/m vs 57 kN/m, but the thickness is much reduced, from 0.51 mm to 0.22 mm. Note also that the Vectran tape was measured to be much weaker in the transverse direction (30 kN/m), so this direction is aligned with the balloon gores to yield the strongest possible joint.

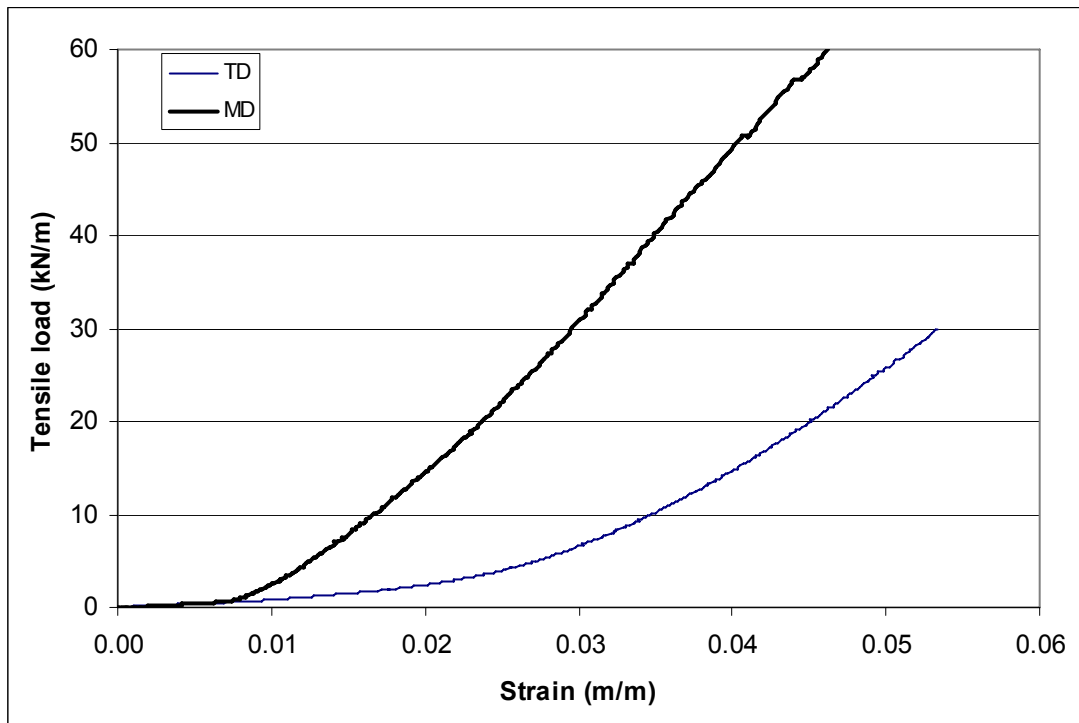


Fig. 1: Load-strain curves for new Vectran structural tapes at room temperature

Additional materials tests were done to assess the creep, relaxation and cyclic effects on the balloon material. Figure 2 shows the creep response for uniaxial specimen exposed to three cycles of load-hold-unload regimen. The test specimens were cut to allow loading along the machine direction. The dimensions of the specimens were 172 mm gauge length and 25.4 mm in width. All testing was conducted on an Instron 8501 Servo-hydraulic machine. In the first testing regimen, the specimen were loaded to 15 KN/m in 40 minutes, held at peak load for 40 minutes, and finally unloaded to nearly zero load in 40 minutes for a total cycle time of 2 hours. During the test, the actuator initial position and displacement was recorded to allow for strain calculations. Upon completion of the first cycle, the loading sequence was repeated twice for a total of three cycles, as shown in the figure. At the end of the three cycles the specimen was taken to break as shown in the last segment of the test. The total duration of the test was a little over six hours. The figure shows a total strain of approximately 2.8% at maximum loading of 15 KN/m, also note the slight creep that occurred during each cycle, as the material is held at the peak load for 40 minutes. Upon gradual load removal during each cycle, the strain was recovered to nearly 1% as shown in the third stage of each cycle. It is also important to note that the total strain did not change significantly as the cycles of loading were repeated.

To assess the ability of the material to recover at higher loads, the test was repeated at higher initial loading of 20 KN/m for two sequences followed by 15 KN for the third sequence (Fig. 3). The duration of each segment, however, was kept the same as the previous test.

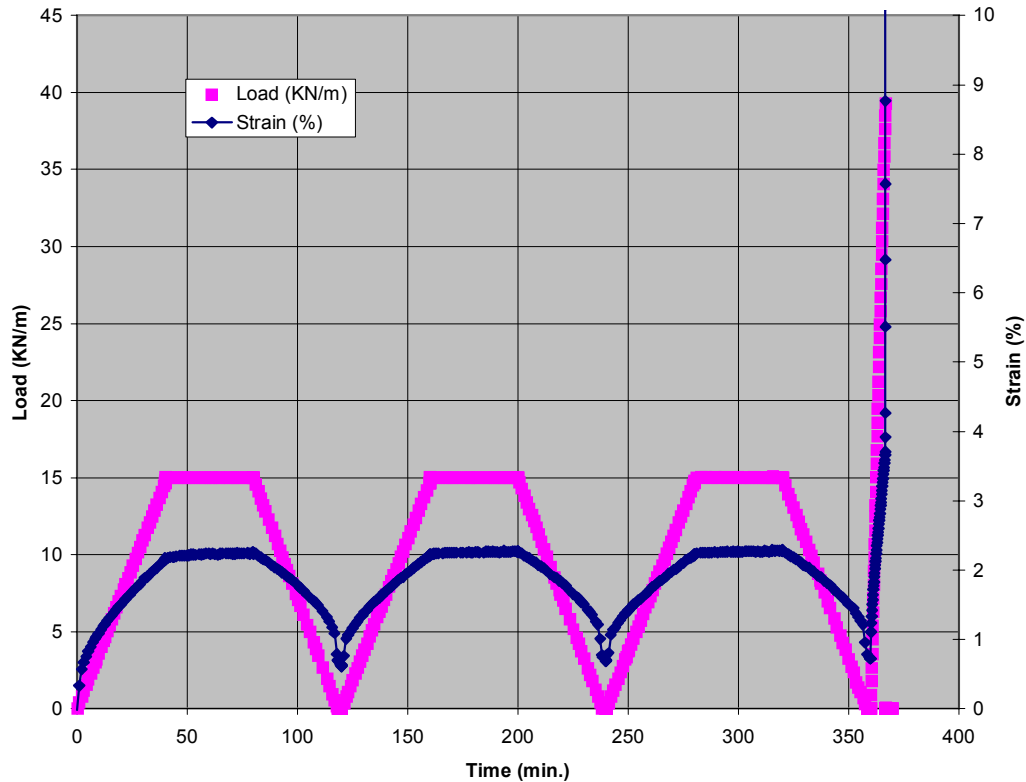


Fig. 2: Strain and recovery response of the balloon material at repeated maximum cyclic loading of 15 KN/m.

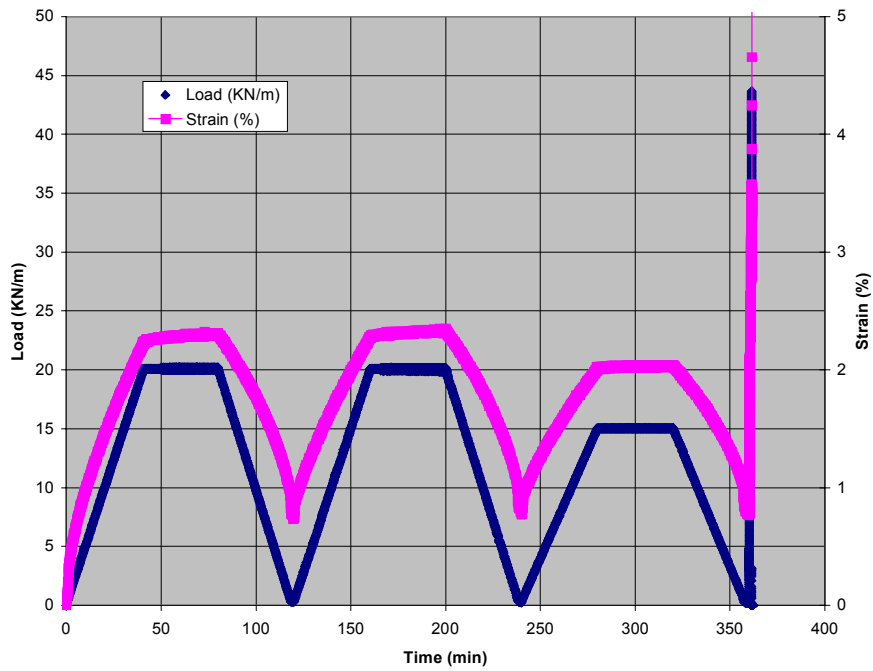


Fig. 3: Strain and recovery response of the balloon material at a combination of maximum cyclic loading of 20 KN/m (2 cycles) and 15 KN/m (1 cycle)

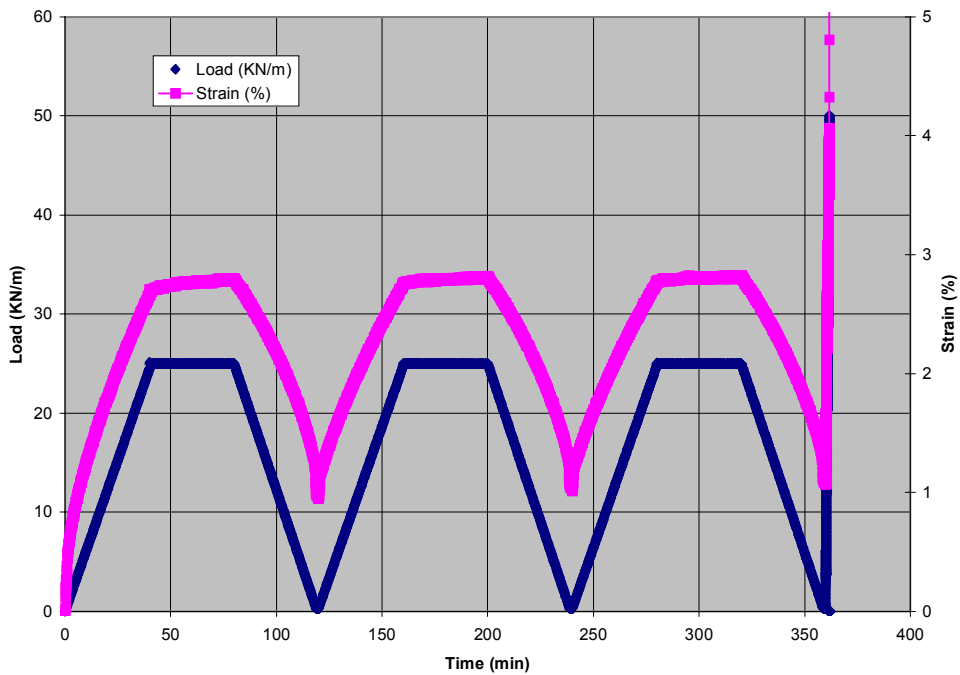


Fig. 4: Strain and recovery response of the balloon material for three cycles at maximum cyclic loading of 25 KN/m.

It is interesting to note that the residual strain at the end of the three sequences was almost identical to that seen at maximum loading of 15 KN/m, indicating little or no effect on the residual strain when the specimen is loaded up to 20 KN/m. Similar results were also obtained when the test was repeated at loading of 25 KN/m (Fig 4).

The viscoelastic behavior of the material was studied further to explore the effect of the number of cycles and duration on the residual strain or strain recovery of the VALOR material. Figure 5 shows a specimen loaded in a similar manner to that shown in Fig. 2 and to a load level of 15 KN/m. However, the duration of each segment was increased to one hour for a total cycle time of 3 hours. The cycles were repeated nine times for a total time of twenty-seven hours. Upon completion of the last cycle, the loading was held to 15 KN/m and the strain recovery was monitored for 24 hours. As shown in the figure, the material recovered from a strain value of 1.5% to approximately 0.4 % in 24 hours. The load was then increased to 20KN/m and the material allowed to recover for another 40 hours reaching a value of less than 0.4% residual strain at the end of the 90 hours test. The stability of the material shown upon loading to relatively high loading levels and the strain response to cyclic loading and recovery reflects the dimensional stability of the composite and the suitability for the planned long duration mission.

Measurements were made on small (~10 cm x 10 cm square) samples of the balloon material to quantify its optical properties on the outer second surface metallized Teflon surface. Data was generated by Optical Data Associates (ODA) with limited cross-checking by JPL, as noted in Table 1. Both unwrinkled and wrinkled samples were tested to assess the impact of handling on the material. Note that the “wrinkled” sample was very heavily wrinkled by hand to

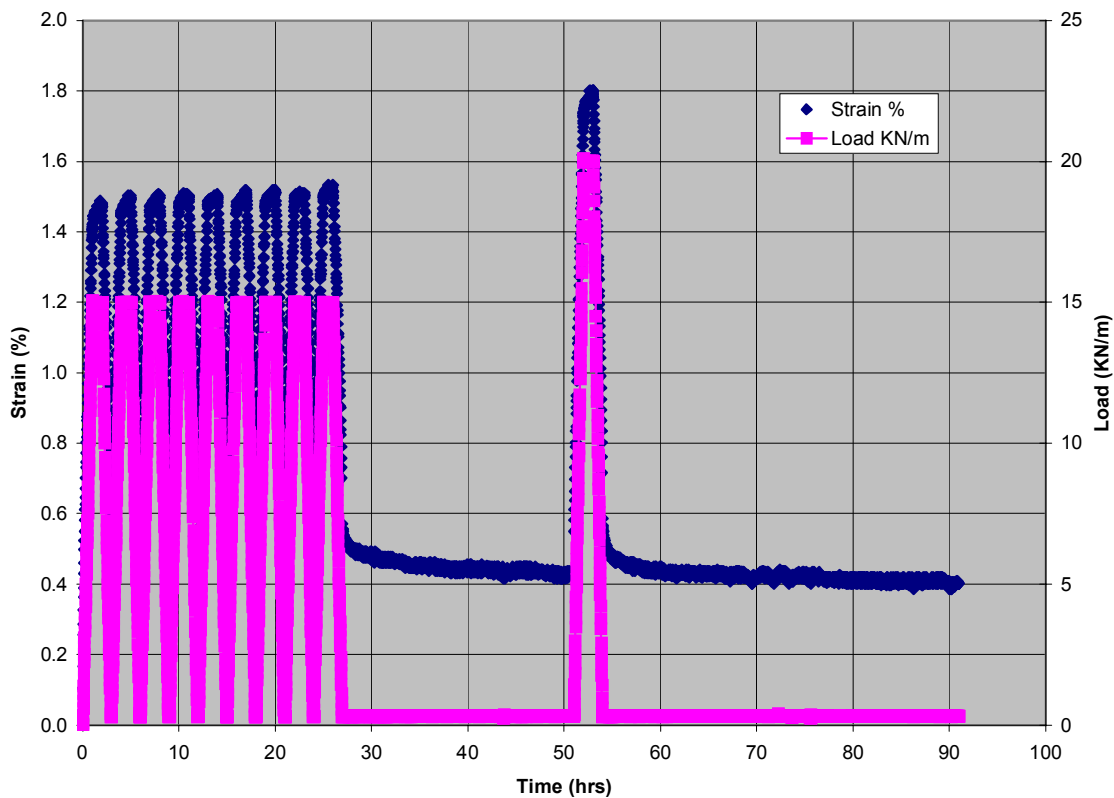


Fig. 5: Repeated cyclic and relaxation response of the balloon material at 15 and 20 KN/m.

a level beyond that which we expect an actual balloon to experience, while “unwrinkled” still has some wrinkling as a result of handling from manufacture and packaging for shipment. It can be seen in Table 1 that there is little or no effect of wrinkling on the IR emissivity measurements. However, wrinkling decreases the solar reflectivity measurement by 6% and increases the solar absorptivity measurement by approximately 40%. Visually, we see that the highly wrinkled material sample shows cracking of the metallized layer, leading to less reflectivity and increased transmission.

The data in Table 1 show that ODA and JPL have reasonable agreement on the solar absorptivity measurement, but do not agree on the infrared (IR) emissivity measurement. However, ODA acknowledges that their apparatus cuts-off part of the relevant IR spectrum and therefore their value will be low. Published data from Gilmore et al (1994) for metallized Teflon shows an IR emissivity of 0.52, very close to the JPL data. Therefore, the selected value for balloon modeling was chosen to be the JPL data point.

Table 1: Balloon Material Optical Property Data

| Condition                 | Tester | Solar reflectivity | Solar absorptivity | IR reflectivity | IR emissivity |
|---------------------------|--------|--------------------|--------------------|-----------------|---------------|
| Unwrinkled                | ODC    | 0.862              | 0.138              | 0.606           | 0.394         |
| Unwrinkled                | JPL    |                    | 0.115              |                 | 0.515         |
|                           |        |                    |                    |                 |               |
| Wrinkled                  | ODC    | 0.808              | 0.192              | 0.618           | 0.382         |
| Wrinkled                  | JPL    |                    | 0.165              |                 | 0.515         |
|                           |        |                    |                    |                 |               |
| Value chosen for modeling |        | 0.81               | 0.15               | 0.61            | 0.51          |

Helium permeability measurements were made by Mocon Inc. on samples of the balloon material. As with the optical property tests, permeability measurements were made on both unwrinkled and wrinkled samples to gauge the effects of severe folding and handling. The results are summarized in Table 2 along with comparison reference data from Dupont on unmetallized Mylar film. As expected, the unwrinkled Venus balloon material shows much lower permeability (factor of 15-20) compared to simple Mylar film as a result of the Mylar metallization as well as the additional metallized Teflon layer. The other notable result is that heavy wrinkling results in a 2.6 factor increase in permeability at room temperature, and a 4.7 factor increase at 50 °C. We believe that the cracking of the metallization layers due to severe folding is the reason for this increase in permeability. The reason for different increases at different temperatures is not known, but may reflect differences in the amount of metal layer cracking rather than a temperature effect per se.

The impact of these permeability data on the predicted balloon lifetime at Venus is fairly benign. Using the unwrinkled value at 50 C results in a loss of 0.07 kg of helium over a 30 day mission, while the wrinkled value at 50 results in an 0.46 kg loss. In neither case will this helium leakage result in a loss of superpressure at the end of a 30 day mission.

Table 2: Balloon Material Permeability to Helium

| Condition                     | Temperature<br>(°C) | Permeability<br>(cm <sup>3</sup> /m <sup>2</sup> -day) |
|-------------------------------|---------------------|--|
| Unwrinkled                    | 23                  | 253  |
| Unwrinkled                    | 50                  | 662  |
| Wrinkled                      | 23                  | 860  |
| Wrinkled                      | 50                  | 4009   |
| Reference data from Dupont:   |                     |  |
| Non-metallized, 12.7 μm Mylar | 23                  | 5580   |
|                               | 50                  | 11780  |

### Prototype 1 Results

Buoyancy measurements conducted on Prototype 1 over a 13.5 day period revealed no leakage in the as-received condition (Hall et al, 2007). Three subsequent experiments were performed on this prototype after that original leakage test:

1. A 3.5 month folding and storage test.
2. A deployment experiment in the laboratory.
3. A sulfuric acid immersion test.

Results from these three tests will now be described.

In August 2006, the prototype balloon was aggressively packaged into an annular volume that approximated that expected for a trip to Venus on an actual mission. Fig. 6 shows a similarly packaged balloon from just before the deployment experiment to be described shortly. Approximately dimensions on the annulus were 0.5 m inner diameter, 1.2 m outer diameter and 0.5 m height. The balloon was wrapped in a spool-like fashion around the inner boundary from one end to the other, with the individual gores longitudinally folded on top of one another. The balloon was stored at the JPL aerobot laboratory for 3.5 months in this configuration with no attempt made to regulate the temperature or humidity. This 3.5 month period roughly corresponds to the expected time of flight from Earth to Venus on an actual mission.

After this storage test, the balloon was re-inflated and monitored for leakage over a 12 day period. This time, a steady loss of buoyancy was detected, from which a total leak was deduced of 0.3 kg of helium, or 2.1% of the total gas charge. This leak was small enough that it did not cause the balloon to lose all of its superpressure in 12 days. Attempts to locate the actual source of the leak on the balloon were not successful despite exhaustive attempts using electronic helium leak detectors. The conclusion was that the folding and handling of the balloon since the first inflation test introduced a small pinhole leak in the balloon, but this could not be proven given our inability to locate the leak itself. The lesson learned from this was to give the balloon more packaged volume and not require such aggressive folding in the future.



Fig. 6: Packaged balloon before drop test



Fig. 7: Successfully deployed balloon

The deployment test was conducted at JPL from this packaged condition. A simple gravity deployment scheme was used in which the balloon was anchored to the top of the drop tower and a simulated 37 kg payload mass at the bottom pulled the bottom of the balloon downwards until the full length was achieved. Total drop distance was approximately 9 meters. Ripstitch was used at the bottom of the balloon to mitigate the transient stress load and dissipate kinetic energy from the drop. The measured peak force in the balloon was 1800 N, approximately 20% lower than predicted based on JPL's ripstitch model. Post drop inspection of the balloon revealed no structural damage (Fig. 7).

The final test performed on Prototype #1 was a sulfuric acid immersion test. The actual experiment did not attempt to submerge the entire balloon, primarily because of safety concerns with handling that much acid. A compromise was implemented in which only one end of the balloon was immersed, consisting of the metal end fitting, the reinforced fabric region around the fitting, and approximately a 1 meter length of adjacent balloon gores. One complication was that

the balloon and its trapped air inside floated in the sulfuric acid; therefore, a metal weight had to be placed on the balloon to keep it submerged. Fig. 8 shows a view looking down into the acid during the experiment.

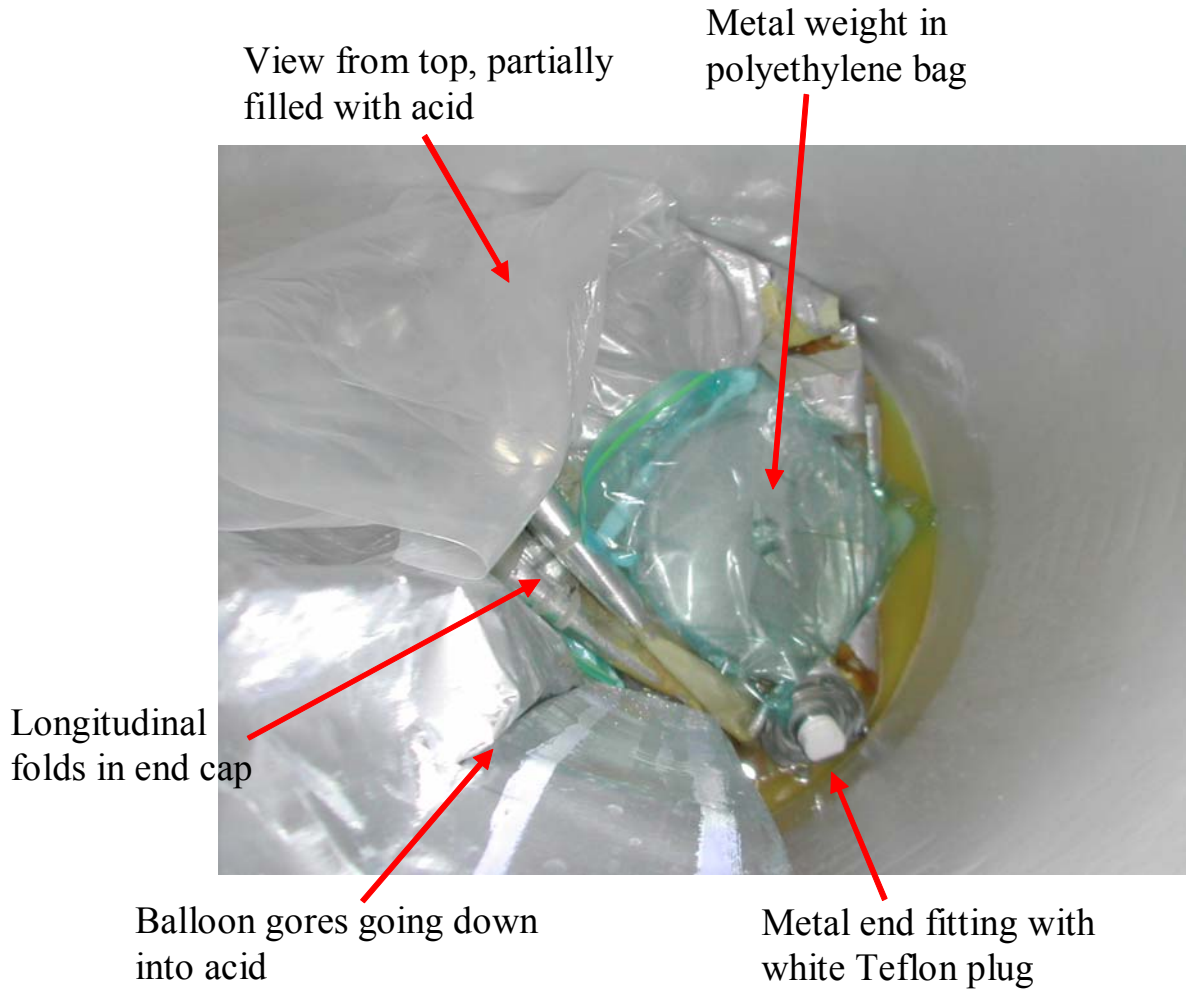


Fig. 8: View of balloon in acid container during immersion test.

No changes in the balloon or the acid bath were observed for the first 5 hours of the experiment. However, between hours 5 and 6 a slight yellowish-brown discoloration was detected. At this point the JPL staff went home for the night. When they returned the next day, the acid bath had a very noticeable brown color (Fig. 8) and it was clear that the balloon itself had been damaged. The acid was drained later that day, the balloon was washed and the inspection began. Total immersion time was approximately 24 hours.

The balloon was badly damaged by the acid. Inspection showed that the acid had penetrated inside the balloon from where it proceeded to dissolve essentially all of the Mylar film and internal polyurethane coating it came into contact with. Also, virtually all exposed gore to gore seams were damaged and delaminated. The Teflon, Vectran and Inconel fitting components appeared to be undamaged.

Extensive analysis was performed on the remnant of the balloon, plus numerous laboratory acid immersion tests on material samples were performed as will be described in the next section. The final conclusion was that the design of the gore-to-gore seams contained a flaw that led to the failure. Specifically, the design used a metallized Teflon cover tape on each seam to protect the balloon from sulfuric acid penetration (Fig. 9). However, the adhesive bond between the metal surface of the tape, the ILC glue and the underlying Teflon gores was not very strong and easily peeled when relatively small forces were applied. Subsequent lab testing showed that the ILC glue provided a very strong joint when applied directly to Teflon film itself, but that the metallization could be very easily peeled off the Teflon. This flaw was exacerbated by the fact that the cover tape has an exposed edge at which the exposed metallization can be directly attacked by sulfuric acid, weakening it further still. We believe that the stresses imposed on the gore-to-gore seams from the folding and, particularly, from the weights placed on the balloon to keep it submerged, eventually led to a peeling of one cover tape in the immersion test and the rapid introduction of acid into the seam and thence into the balloon itself. Prior laboratory testing at JPL on seam samples did not impart any peeling force on the joint and therefore did not find this failure mechanism (Hall et al, 2007). It is arguable that the actual flight balloon will not experience this kind of peeling force in the Venusian atmosphere; nevertheless, a fix to this design flaw was quickly found and implemented, as will be described in a later section of this paper.

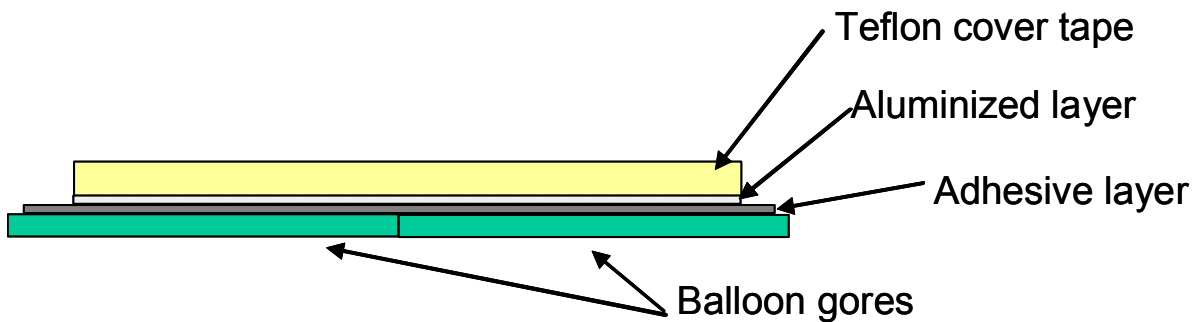


Fig. 9: Schematic diagram of flawed gore-to-gore joint

### Additional Material Sulfuric Acid Testing

A new set of laboratory acid exposure tests were conducted in the aftermath of the Prototype #1 immersion test. The first set of new tests were conducted on Mylar film by itself. Previous work (Hall et al, 2007, Table 4) reported that Mylar film by itself tolerated up to 85% concentration sulfuric acid at 70 °C for two days. However, as was described above, the immersion test with the actual balloon at 85% concentration and room temperature resulted in destruction of the Mylar wherever it was exposed. This contradiction was resolved by new room temperature exposure tests. The new results showed that Mylar film tolerated 75% concentration at room temperature for at least 5 days, but that higher concentrations resulted in Mylar damage, with the damage occurring slowly at 80% and very quickly (i.e., in minutes) at 85% concentration. The prior result in 2006 was evidently in error perhaps due to errors in the concentration measurement of the acid in those earlier tests. The conclusion is that Mylar will

not form a secondary acid barrier in case the Teflon is breached unless the acid concentration is 75% or less.

The next acid experiment consisted of 85% concentration exposure over 8 days to a pair of balloon material samples cut from previously unexposed gores of Prototype #1. A region of highly wrinkled material was selected for this purpose, and then one of the samples was folded many more times by hand to give it an “extra tortured” character. Despite this rough handling, however, neither sample showed any acid penetration to the backside over the 8 day test (Fig. 10). This result illustrates the robust character of the outer Teflon layer.



Fig. 10: Acid-tested samples from Prototype #1 balloon

Seam testing was performed next. Both an original seam (Fig. 9) and a “backwards” seam with metallization on top of the cover tape were tested at 85% concentration. The result (Fig. 11) clearly showed that the acid ate its way in from the free edge of the original seam, whereas the backwards seam lost its surface metallization but no damage was done to the glued joint between the Teflon cover tape and the Teflon gores. This provides more direct evidence for the plausibility of the seam failure mechanism described above for the immersion test.

These results convinced us that the seam design had to be modified so as to not have the metallization on the cover tape and thereby ensure a strong, acid resistant adhesive bond between the Teflon cover tape and Teflon gores. ILC Dover constructed a sample joint with this new design and sent it to JPL for acid immersion testing. This sample was exposed to 85% concentration (rising to 92% concentration by the end due to unexpected removal of water from the acid) and 70 °C temperature for 33 days and showed no penetration of the acid to the backside of the material. However, the acid did take on a yellowish color after 12 days, and there was some point-like discoloration of the exposed adhesive (Fig. 12). Also, small bubbles were

seen in the acid pool on the surface of the material. We concluded that a very slow chemical reaction was occurring between the acid and the adhesive, but that it was not serious enough to cause a failure under these aggressive acid exposure conditions. It was on this basis that the new seam design was selected for Prototype #2.

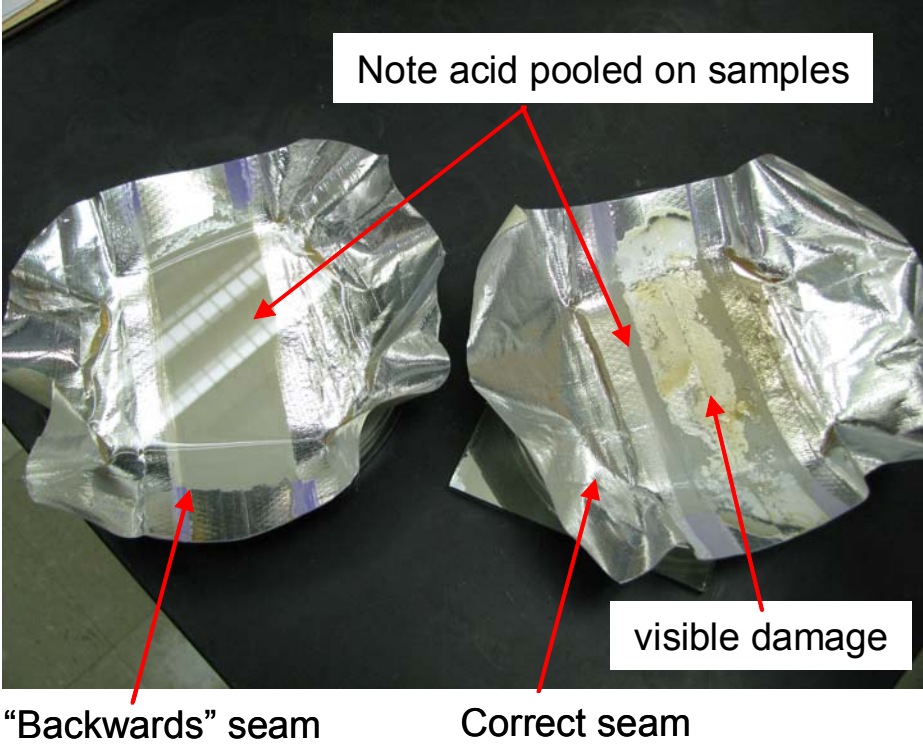


Fig. 11: Acid exposure results on seam samples



Fig. 12: New seam after 33 day acid immersion

### Finite Element Analysis

The tensile strength of the gore material in Prototype #1 was reported to be 57 kN/m in the fill direction and 71 kN/m in the warp direction (Hall et al, 2007, Table 3). Subsequent testing done at the NASA Wallops Flight Facility yielded a slightly lower strength of 52.1 kN/m in the fill direction. On the basis of thin membrane theory, the pressure that would generate this loading in the fill direction would be

$$P = \frac{2(\sigma t)}{r} = \frac{2(52100)}{2.75} = 37,890 \text{ Pa} \quad (1)$$

However, it is expected that departures from thin membrane theory would in fact occur given the non-linear, anisotropic nature of the balloon laminate material, the flat gore construction and the presence of a 45 kg load on the bottom fitting. Finite element analyses of the balloon were therefore performed to predict the stress distribution and thereby quantify departures from thin membrane theory. This in turn allows for the computation of the overall structural safety margin for the balloon during Venusian flight.

Prior work on finite element modeling of Mars balloons showed good results using the LS-DYNA a commercially available explicit finite element code (White and Day, 2003). Therefore, this software was selected for this Venus modeling task. The explicit method permits stable solution of fabric structure problems, in contrast to standard implicit codes dependent on stiffness equations. LS-DYNA includes a fabric material type with orthotropic material properties and tension-only behavior, as well as a layered composite shell that permits arbitrary material orientations. The analysis method in LS-DYNA is a non-linear, time-dependent dynamic simulation. Since static stress results were desired, a relatively slow rate of loading was

employed in ramped stages. After each level of loading, damping was applied to smooth out noise (vibrations) in the response. The geometry of the balloon was generated in an initial, unstressed state with segmented panels (gores). Pressure was then applied incrementally, inflating the vessel. After initial inflation to 1000 Pa, at which point the balloon had some structure, payload and body forces were added, simulating the buoyant force. Internal pressurization was then continued to a load level of 20,000 Pa. One-eighth geometrical symmetry was assumed to reduce the size of the computational problem.

Nonlinear material behavior was specified through the use of uniaxial material curves in each of three material directions -- warp, fill and 45° (shear) direction. The material curves were obtained by testing samples of the balloon envelope and load tape materials. Seams were modeled using material curves from composite sample test results, and the end cap region was modeled using a composite, layered shell. Stress-strain, thickness and tensile strength data for these materials were presented above in the materials testing section.

A large number of simulations were performed on the Prototype #1 design, various options for the Prototype #2 design, and other simplified test cases. This paper will present some results on the simulation of the final Prototype #2 design and briefly discuss some aspects of the other simulation results that led to the design choices made. The changes made between the first and second prototypes are summarized in the next section below.

The main finding was that the Venus balloon had two regions of stress concentration that elevated significantly above the thin-membrane limit. One region was in the fabric end cap immediately adjacent to the junction with the metal fitting; the other region was in the gores at the three-way junction of the gore, the end cap and the structural tapes on either side of the gore. Figure 13 presents a von Mises stress plot that shows the end cap stress concentration, and Fig. 14 presents a von-Mises stress plot that shows the gore stress concentration.

There are two end cap stress concentration points as seen in Fig. 13. The peak von Mises stress is 329 MPa which, given the 3 layer construction of thickness 0.507 mm, corresponds to a force per unit width of 166.8 kN/m. This is substantially higher than the thin membrane value ( $\sigma$ ) of 27.5 kN/m. Given that each Vectran layer of the end cap has an ultimate tensile stress of approximately 340 MPa, the simulation pressure of 20,000 Pa corresponds to the very close to the failure point despite being at roughly half of the thin membrane burst pressure prediction (Eq. 1) and having three layers of material in the end cap. The cause of the stress concentration appears to be related to the anisotropic nature of the Vectran fabric that makes up the end cap. Simulations performed with uniform thickness isotropic material show only a 29% increase in stress near the metal fitting, evidently arising from the stiffness mis-match between the balloon material and the metal at the boundary. The aligned nature of the Vectran threads in warp and fill directions combined with the high stiffness of those threads therefore leads to much higher stresses at the points shown in Fig. R. Note that the one of the Vectran layers is oriented at 45° to the other layers in an attempt to mitigate the anisotropy. Also, the end cap balloon material is modeled as having a clamped boundary condition at the metal at the metal junction.

It is unclear how this very high stress will manifest itself in the real structure at high loads. It would not take much plastic deformation of the material at these points to relieve the stress, whether or not this would result in a macroscopic balloon failure is not known. An obvious design change that can be considered in the future is to replace the 3 layer Vectran construction with many more thinner layer so as to better approach the isotropic ideal limit that has much reduced stresses.

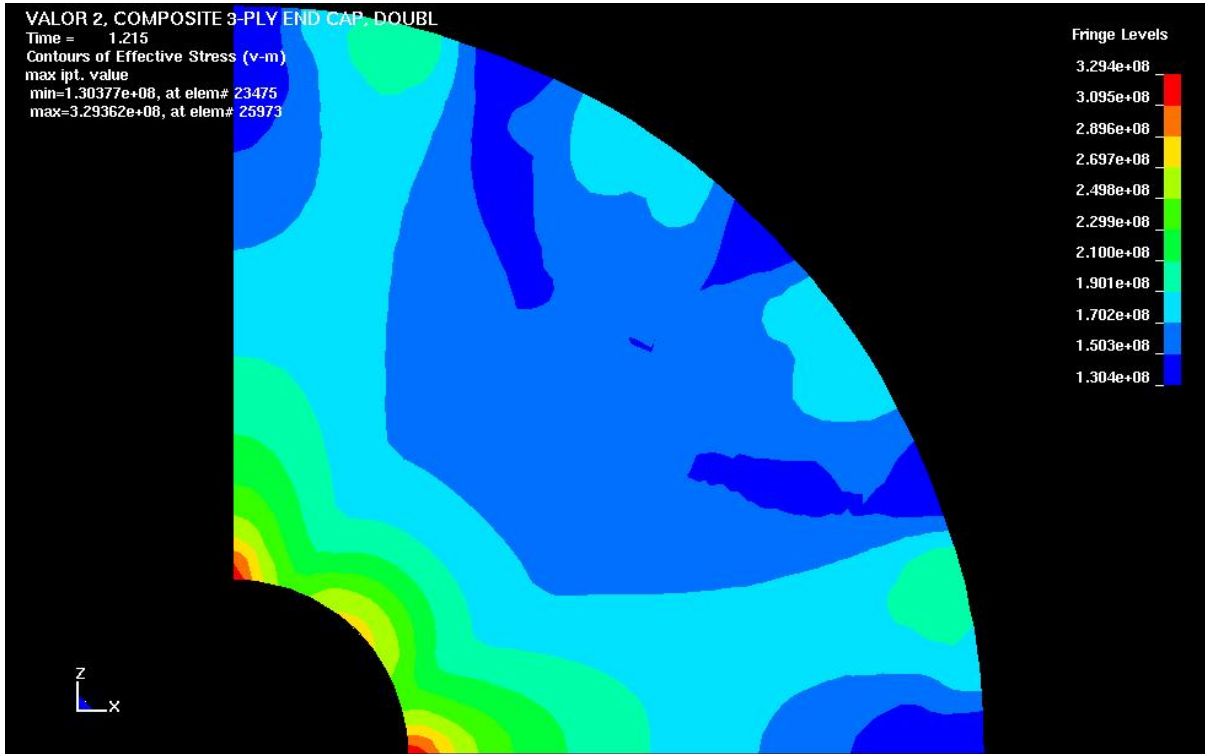


Fig. 13: Plot of von Mises stress in balloon end cap, Prototype #2 design at 20000 Pa of internal pressurization. The units on the color bar are Pa.

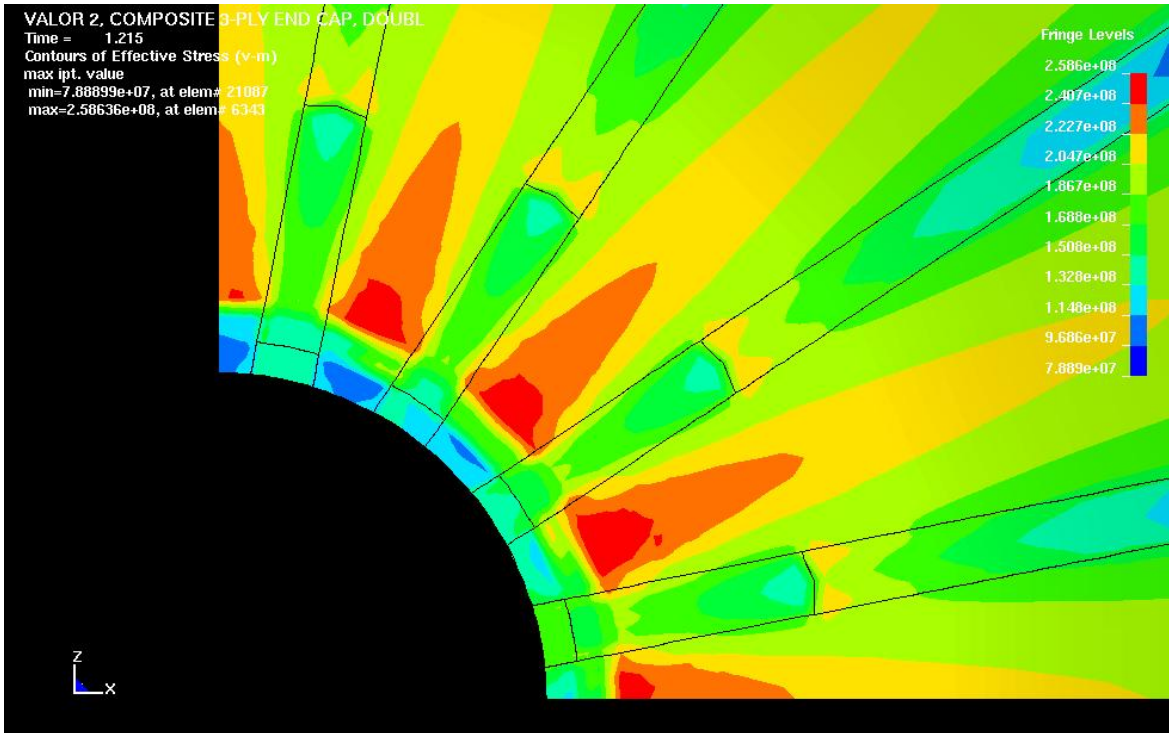


Fig. 14: Plot of von Mises stress in balloon gores and tapes, Prototype #2 design at 20000 Pa internal pressurization. The units on the color bar are Pa.

The gore stress concentration shown in Fig. 14 results from the stiffness mismatch between the relatively thin gore and the much thicker and stiffer end cap and adjacent structure tapes. Note that the structure tapes are doubled-up for a short 20 cm length on each gore-to-gore junction (there is a black line in each tape denoting the end point of the doubling), a design feature that eliminates a similar stress concentration seen in the structure tape itself in this region. The peak stress seen is 259 MPa, compared to a thin membrane value of 169 MPa given a 20000 Pa pressurization. This is an increase of 53% over the thin membrane limit.

Table 3 summarizes the computed peak stresses at 20,000 Pa pressurization, along with the ultimate tensile strength of each element and the predicted failure pressure. These results show that the end cap will fail first, soon followed by the seams and lastly by the gores. The direction for the future is to improve the end cap performance through a more isotropic construction of the fabric material and strengthen the seams to equal or exceed the failure pressure predicted for the gore material itself.

Table 3: Prototype #2 FEA Simulation Summary

| Element | Thickness (mm) | Ultimate tensile strength (MPa) | FEA peak stress result (20kPa pressurization) (MPa) | Predicted balloon failure pressure (Pa) |
|---------|----------------|---------------------------------|---|---|
| Gore    | 0.163          | 320                             | 259   | 24,500                                  |
| Seam    | 0.338          | 263                             | 251   | 21,000                                  |
| End cap | 0.507          | 320                             | 329   | 19,500                                  |

## Prototype 2 Design

The accumulated information described above from the Prototype #1 fabrication and testing, the laboratory materials testing and the finite element analysis, led to a small set of design changes that were incorporated into Prototype #2. These are summarized as follows:

1. Replacement of polyester fabric-based load tapes with new Veteran-based load tapes. The use of Veteran allows for a much thinner (0.22 mm vs 0.54 mm) tape with equivalent strength.
2. Add 32 strips of load tape at each gore-to-gore joint, 16 at the top and 16 at the bottom, to provide a 20 cm long doubling of the load tape at the end cap reinforcement region. As described above, this reinforcement serves to reduce the stress concentration observed in the gore at the junction with the end cap.
3. Use a two-part Teflon cover tape. The inner tape is non-metallized to ensure a strong adhesive bond between the cover tape and gore. The outer tape is metallized as in Prototype #1 and is included to provide better optical properties (absorptivity and emissivity) and better aesthetics. Analysis indicated that even if this tape was damaged by sulfuric acid exposure, the resulting increase in balloon heating would be just a few degrees.
4. Increase the diameter of the Inconel end fitting from 8.9 to 15.2 cm in diameter. This provides a wider distribution of stress from the payload weight.

## Prototype 2 Fabrication and Test

Fabrication of Prototype #2 proceeded normally. All patterned parts were marked and cut on ILC's automated wheel cutting table. Gores and end caps then had ILC adhesive manually applied (painted on) to an approximately width of 23 mm around their perimeters. All cover tapes, both FEP film and aluminized FEP film, were completely painted on the appropriate side with primer and adhesive. Gores were then joined by thermal welding, per seam construction shown in Figure 1.

The end cap assemblies were fabricated by thermally welding their constituent layers. Once sealed together, the center hole pattern for the inflation fitting was cut. End fitting assemblies were then installed, starting with the epoxy bonding of the diffuser/clamp ring to the interior face of the end cap. The Hastelloy inflation fitting with Viton o-ring and gasket was then attached to the exterior of each end cap with twelve 4-40 UNC A286 flathead screws. Once installed, the fittings were covered in padding to ensure that they did not damage the surfaces of the FEP envelope during subsequent assembly operations. With only a portion of the final gore seam left open, the end cap assemblies (with hardware) were thermally welded into the assembled gores. The final length of gore seam was then thermally welded, completing the envelope. A photograph of the finished balloon is shown in Fig. 15 during the initial leak test at ILC Dover.



Fig. 15: Inflated balloon Prototype #2 during leak check at ILC Dover

The balloon was sent to JPL and then inflated for a long duration buoyancy and leak check. The change in superpressure over time is plotted in Fig. 16, compared to a “no leak” superpressure that has the effects of atmospheric pressure and temperature changes subtracted out. As can be seen, the superpressure time history does not show a large divergence from that expected by changes in the environment, indicating a low to negligible level of leakage.

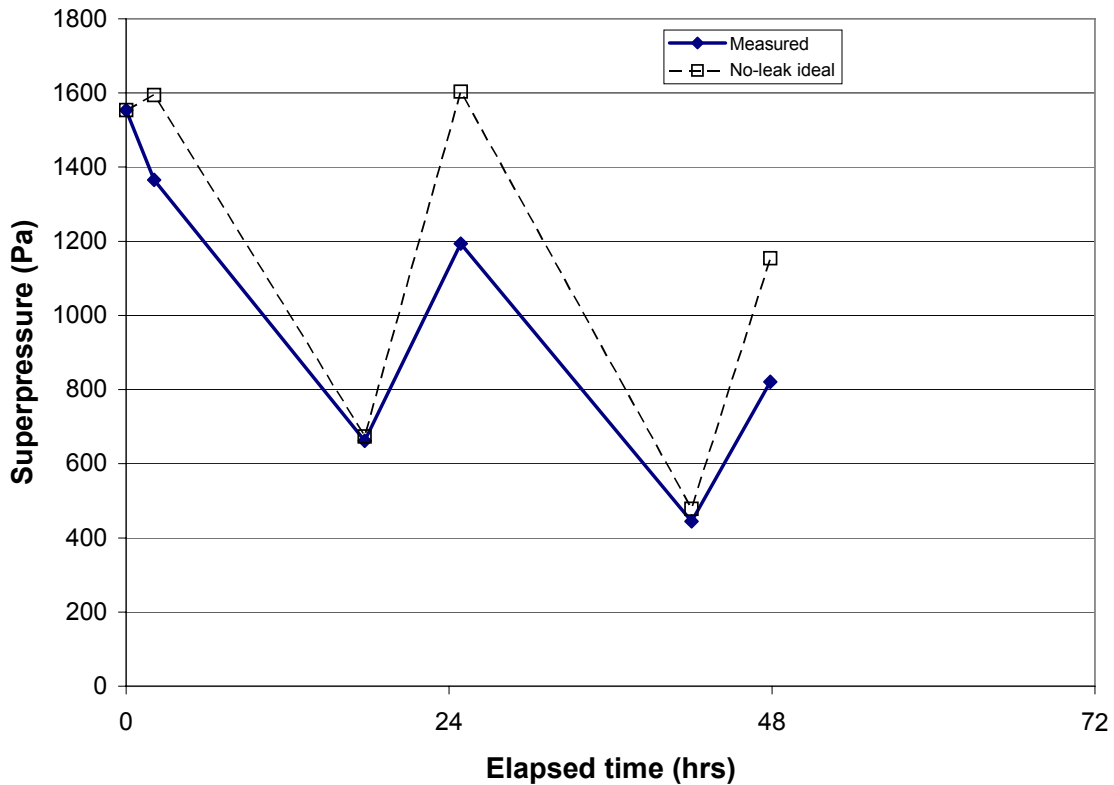


Fig. 16: Prototype #2 superpressure versus time

## Conclusions

A second generation Venus prototype balloon was designed, fabricated and tested. This new balloon incorporated lessons learned from the original prototype, along with extensive laboratory testing on the material properties and finite element analyses of the balloon structural performance under load. The result is an improved balloon with much better characterized properties and improved confidence in its ability to succeed in an actual flight mission in the Venusian environment.

## Acknowledgements

The research described in this paper was performed at the Jet Propulsion Laboratory, California Institute of Technology, NASA Wallops Flight Facility and ILC Dover Inc., under a contract with the National Aeronautics and Space Administration. We would like to thank Eric Kulczycki of JPL for his help in performing the Prototype #2 inflation experiment. We would also like to thank Optical Data Associates and Mocon Inc. for their help in making the balloon material optical property and permeability measurements respectively.

## References

- David G. Gilmore (ed) (1994). "Satellite Thermal Control Handbook", The Aerospace Corporation Press, El Segundo, CA. See page A-6, 1 mil Teflon with gold backing,  $\epsilon = 0.52$ .
- J. L. Hall, D. Fairbrother, T. Frederickson, V. V. Kerzhanovich, M. Said, C. Sandy, C. Willey and A. H. Yavrouian, (2007). "Prototype design and testing of a Venus long duration, high altitude balloon", *Advances in Space Research*, (in press, available online at <http://www.sciencedirect.com/>).
- Kremnev, R. S., Linkin, V. M., et al, (1986). "Vega Balloon System and Instrumentation," *Science*, v.231, p. 1408-1411.
- White, C. and Day, S. (2003). "Analysis and Experimentation for the Aerial Deployment of Planetary Balloons", IEEE Aerospace Conference, Big Sky, MT, March 9-14, 2003.